ORIGINAL RESEARCH ARTICLE

# Cyclic Phase Transition-Assisted Spark Plasma Sintering of AlCoCrFeNi Complex Concentrated Alloys

RUNJIAN JIANG, ELISA TORRESANI, ANDRII MAXIMENKO, HAOREN WANG, SABINE FAULHABER, KENNETH VECCHIO, and EUGENE A. OLEVSKY

This paper is devoted to achieving accelerated densification, optimized microstructure, and improved mechanical properties of AlCoCrFeNi complex concentrated alloys (CCAs) by applying cyclic phase transition (CPT) process in spark plasma sintering (SPS) at low temperature. Scanning electron microscopy (SEM) and electron backscatter diffraction (EBSD) were performed to correlate the sintering shrinkage with associated microstructural changes. Experimental results show that CPT process promotes the formation of refined intragranular BCC/B2 structure and networked dendritic FCC phase at grain boundaries in the CCAs. The proposed CPT-assisted sintering not only promotes these CCAs to have a fully dense structure that is unobtainable in regular sintering at lower-limit temperature (800 °C), but also promotes these CCAs to have an accelerated densification that does not exist in regular sintering at upper-limit temperature (1000 °C). This better densification outcome is contributed by distinctive elemental redistribution and nano-grain clusters, which promote the mass transfer and the superplasticity behavior in the CCAs. Given this, hardened BCC phase (471HV) and softened FCC phase (188HV) can be obtained in AlCoCrFeNi CCAs after CPT-assisted sintering, which brings a synergistic effect to overcome the strength–ductility trade-off in CCAs. This work is expected to provide more insights into the efficient sintering of complex alloys.

https://doi.org/10.1007/s11661-024-07308-9


## I. INTRODUCTION

HIGH-ENTROPY alloys (HEAs) have emerged as one of the topics in the spotlight of physical metallurgy, since their concept was first proposed two decades ago.[1,2] Complex concentrated alloys (CCAs) are a broader class of alloys compared to HEAs, allowing for the alloys with multi-phase structure. Compared with conventional dilute alloys, CCAs tend to generate a single or multiple solid solution structures with excellent mechanical and functional properties.[3–6] Even though the kinetically slow diffusivity rate induced by high configuration entropy can bring the alloys with simple BCC and/or FCC structure, it does not mean that the acquisition of such ideal microstructure in CCAs is always undertaken effortlessly in a carefree manner. Powder-based metallurgy (or sintering[7]), as a solid-state manufacturing route, can prepare bulk CCAs by the consolidation of pre-alloyed or mechanically alloyed powders below their liquidus temperature. It brings better compositional uniformity in CCAs than other common processing route, including casting, which requires multiple smelting processes to improve the mixing of individual elements.[8] The grain growth and microstructure change during solidification also need to be considered.[9] Nevertheless, the sintering of CCAs still should address achieving fast and satisfactory densification,[10] even though the sluggish diffusivity effect, considered as an attribute of CCAs, is controversial.[11,12] The pursuit of better densification behavior in sintered CCAs should be motivated by the acquisition of their high strength and modulus,[13–15] but many will only be achieved by sintering at high temperature.

RUNJIAN JIANG is with the Department of Mechanical Engineering, San Diego State University, San Diego, CA 92182 and also with the Department of Mechanical and Aerospace Engineering, University of California San Diego, La Jolla, CA 92093. ELISA TORRESANI and ANDRII MAXIMENKO are with the Department of Mechanical Engineering, San Diego State University. HAOREN WANG, SABINE FAULHABER, and KENNETH VECCHIO are with the Department of NanoEngineering, University of California San Diego, La Jolla, CA 92093. EUGENE A. OLEVSKY is with the Department of Mechanical Engineering, San Diego State University and also with the Department of NanoEngineering, University of California San Diego. Contact e-mail: eolevsky@sdsu.edu
Manuscript submitted June 19, 2023; accepted January 2, 2024.
Article published online February 13, 2024

The alloy grouping composed of AlCoCrFeNi elements has been one of the most studied systems in the CCAs family tree which is utilized in high temperature environments due to its good oxidation resistance and mechanical properties.[16,17] The BCC/FCC dual-phase microstructure with desired density in AlCoCrFeNi-type CCAs generally requires spark plasma sintering (SPS) process at about 1200 °C, not far from their melting point (~ 1350 °C).[18–21] For some refractory HEAs, higher sintering temperature and longer holding time are the preference for better densification.[22–24] The regular sintering route for these CCAs referred to as a common sintering way, where only time, of all processing parameters, changes during the isothermal stage, is not only energy-consuming but also has the risk of grain coarsening. It gives sintered alloys an eclipsed structural diversity in consideration of compositional diversity as well. The strategy of thermal cycles was first proposed decades years ago when the accelerated densification in pure iron was observed.[25] The multiple thermal cycles across $\alpha/\gamma$ phase transition temperature were experimentally confirmed to favor a higher final density of the sintered cast iron powders.[26] Such benefit perhaps is associated with the internal stress plasticity produced by anisotropic thermal expansion mismatch and the phase transformation superplasticity produced by transition lattice mismatch.[27,28] Powder consolidation in this case is also accompanied by grain refinement due to the activation of nucleation during recrystallization.[29] Given this constructive effect on the sintering of traditional metals, the thermal cycling coupled with phase transition can be introduced as the extra dimension into the sintering of complex alloys. This cyclic phase transition (CPT)-assisted sintering of CCAs is developed where both the temperature and the phase are adjustable. The CCAs are no longer regarded as single solid solution phase with thermal stability at all temperatures below its melting point.[30,31] CALTHAD analyses of many BCC/FCC dual-phase HEAs or CCAs also show their complex phase compositions and transformations as a function of temperature.[31–33] This undoubtedly opens a possibility to explore the CPT-assisted sintering of dual-phase CCAs. Thermal cycles during or post sintering have already been conducted in some conventional alloys to achieve enhanced properties, but no phase transition process is coupled to demonstrate the microstructure modification or densification improvement.[34,35] Additionally, some studies try to correlate the phase transition behavior with the sintering process of complex alloys, but they are still within the regular sintering framework near the phase transition temperature without applying thermal cycling.[36,37]

In this paper, repetitive phase transformation *via* thermal cycling enables the low-temperature SPS of dual-phase AlCoCrFeNi CCAs with better densification behavior. It is noted that the repetitive phase transitions induced by temperature oscillations in sintering are obviously different from other straight-forward thermal cycle sintering,[38,39] as the microstructural regulation and the densification acceleration are made possible simultaneously. The phase transition between BCC/B2 (800 °C) and FCC (1000 °C) guarantees a feasible CPT-assisted sintering process within the low-temperature range in this dual-phase CCAs.[32] The diffusion behavior on sintering can be improved by repeatedly applying this diffusion-based BCC/B2 and FCC phase transition process.[40] These provide a promising avenue to optimize the microstructure and properties without sacrificing densification in this AlCoCrFeNi CCAs. The proposed sintering process can be generalized to the powder-based manufacturing of all CCAs, especially dual-phase CCAs with phase transition process at sintering-preferred temperature.

## II. EXPERIMENTAL

### A. *Synthesis Process*

The gas-atomized equiatomic AlCoCrFeNi pre-alloyed polycrystalline powders (> 99.95 pct purity; provided by Sino-Euro Materials Technologies, China) were utilized as the raw materials. The powder features in Figure 1 indicate that the CCAs powders have highly pure BCC structure with small amount of residual FCC phase due to fast cooling during gas atomization. Their median particle size is about 85 $\mu$m. The difference of BCC/B2 lattice size by composition uniformity possible leads to the formation of shoulder peak of at 82 deg. Their apparent density and theoretical density are 3.80 and 7.01 g/cm$^3$, respectively. The pre-alloyed AlCoCrFeNi powders were containerized into a graphite mold (30 mm in diameter, 60 mm in height, and 10 mm in inner diameter). The spark plasma sintering device manufactured by SPS Syntex Inc., (Dr. Sinter SPSS-515) was applied to carry out the sintering experiments. The powder samples were separated from tooling by 0.15-mm-thick graphite paper and were compacted under a load of 3 kN to get the green body. The differential scanning calorimetry (DSC) curve of raw powders indicates two phase transition behaviors (Figure 1(c)), among which 958 °C, being sintering-preferred temperature, is the formation temperature of the FCC phase. Above this temperature, considerable FCC phase fraction be obtained in the alloy with the suppression of $\sigma$ phase generation at a high heating rate.[30] For regular sintering, the sample was heated to the prescribed temperature (1000 °C or 800 °C) with a heating rate of 100 K/min followed by isothermal hold of 30 minutes. For cyclic phase transition-assisted sintering, the sample was first heated to 1000 °C with a heating rate of 100 K/min, and then was subjected to the thermal cycles between 800 °C and 1000 °C with local heating and cooling rate both being 100 K/min. In this case, a total of three cycles was applied and in each of

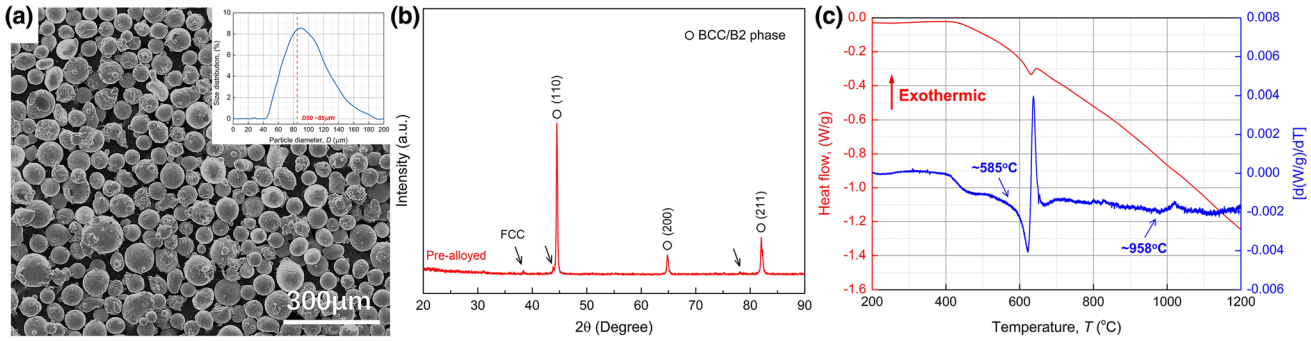


Fig. 1—The characterization and thermal analysis of gas-atomized AlCoCrFeNi CCAs powders: (*a*) SEM image with particle size analysis; (*b*) powder X-ray diffraction (XRD) pattern showing a series of peaks corresponding to BCC structure; (*c*) differential scanning calorimetry (DSC) curve showing the formation of FCC phase at sintering-preferred temperature of about 958 °C (in Argon atmosphere of 100 mL/min).

them, a local hold of 1 minutes at the upper-limit temperature and 5 minutes at the lower-limit temperature were utilized. This is to achieve the energy-saving low-temperature sintering of AlCoCrFeNi CCAs under the premise of sufficient densification. An extra isothermal hold at 800 °C following each of two sintering conditions aims at obtaining the $\sigma$ phase precipitation under the regular and CPT-assisted sintering case. By doing this, a preferred condition of long-time isothermal holding or slow heating rate is confirmed for the $\sigma$ phase formation. Thus, it is evident that the involvement of such $\sigma$ phase in densification can be negligible during the SPS of this AlCoCrFeNi CCAs at high heating/cooling rate. An external axial pressure of 50 MPa was applied throughout all the four sintering processes. The samples with a diameter of about 10 mm and a length of about 12 mm were prepared eventually.

### B. *Characterization*

A group of cylindrical AlCoCrFeNi CCAs samples with a diameter of about 10 mm were obtained accordingly. The relative density of sintered CCAs was estimated by Archimedes method. The Vickers hardness (HV) of samples was measured with a digital microhardness tester at a load of 50 gf and a holding time of 10 seconds. The nano-indentation experiments (G200 Nano Indenter, Keysight) were applied to determine the mechanical properties of BCC/B2 and FCC phases in CCAs under different sintering conditions. The maximum load ranging from 50 to 200 mN and the hold time of 10 seconds were utilized. To find the suitable sintering temperature range for CPT-assisted sintering, the phase transition temperatures of CCAs powders were detected by differential scanning calorimetry (DSC-TGA, SDT-Q600, TA Instruments) with a heating rate of 10 K/min and Argon gas flow rate of 100 mL/min. The phase structures of raw powders and sintered alloys were characterized by X-ray diffraction (XRD) with CuK$\alpha$ radiation (X'pert pro XRD, PANalytical Co.). The Bragg angles were adjusted in the range of 20 to 90 deg for the samples with a scanning rate of 5 deg/min. The microstructure features of raw powders and sintered alloys were observed in field emission scanning electron microscopy (FE-SEM, FEI Apreo, Thermo Fisher) equipped with Oxford Instruments' energy-dispersive X-ray spectrometer (EDS) and an electron backscatter diffraction (EBSD) detector.

## III. RESULTS

### A. *Densification Behavior and Density of AlCoCrFeNi Sintered CCAs*

The FCC–BCC phase transition induced by temperature change can happen in between each local heating or cooling stage. It is shown that AlCoCrFeNi CCAs have an insufficient densification (solid line) and densification rate (dash line) during regular sintering at 800 °C (Figure 2(a)), in which only sintering necks form while no obvious shrinkage happens. This indicates that in the CPT-assisted SPS process, the ideal highly dense structure can still be obtained even if the lower-limit temperature is not sintering-preferred. A comparison of the densification of Alloy A (regular sintering at upper-limit temperature) and Alloy B (CPT-assisted sintering) is given in Figure 3(a). Sample-free sintering process under the same temperature profile has been applied to remove the influence of thermal expansion of graphite tooling on densification measurement. Alloy B apparently obtains a fully dense structure with a relative density of 99.8 pct in contrast to a high but incomplete densification in Alloy A with a relative density of 95.7 pct. In this AlCoCrFeNi sintered CCAs, the density "jump" almost occurs within the first cycle, then considerably weakens in the second one and is almost absent in the third one. Even though the shrinkage caused by each cycle is gradually minimized, the presence of CPT undeniably brings a better manufacturing outcome that surpasses the regular sintering at the upper-limit temperature. The insert curve indicates that most of the densification in sintered CCAs is finished during the initial heating stage, and it is almost stagnant at the isothermal holding stage for regular sintering condition. The detailed inspection in CPT-assisted SPS process informs that the higher densification rate is preferentially caused by local heating and cooling (blue and red portion) within one specific thermal cycle, which is direct evidence for the contribution of this cyclic phase transition to accelerate the densification of

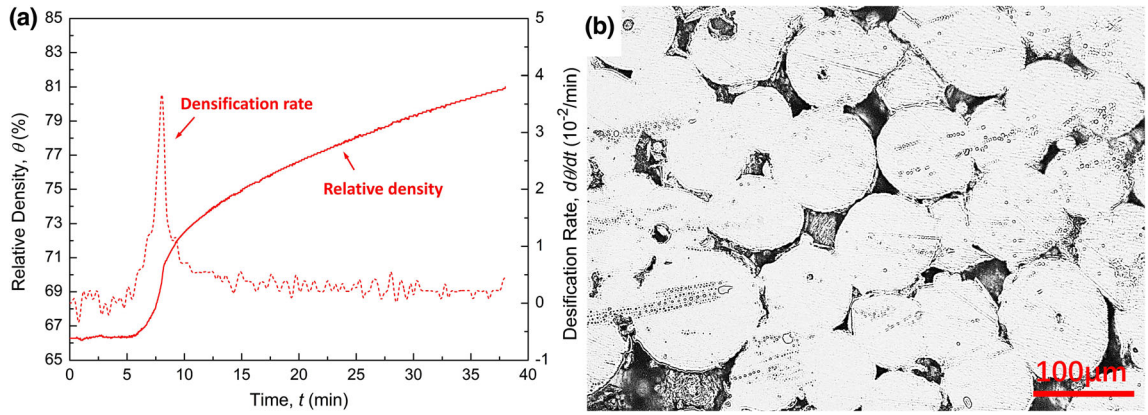


Fig. 2—The densification and morphology of AlCoCrFeNi CCAs by regular sintering at lower-limit temperature (800 °C): (*a*) densification curve (solid line) and densification rate curve (dash line) showing an unsuccessful sintering outcome and a low densification rate; (*b*) optical microscope image showing insufficient shrinkage with only neck formation.

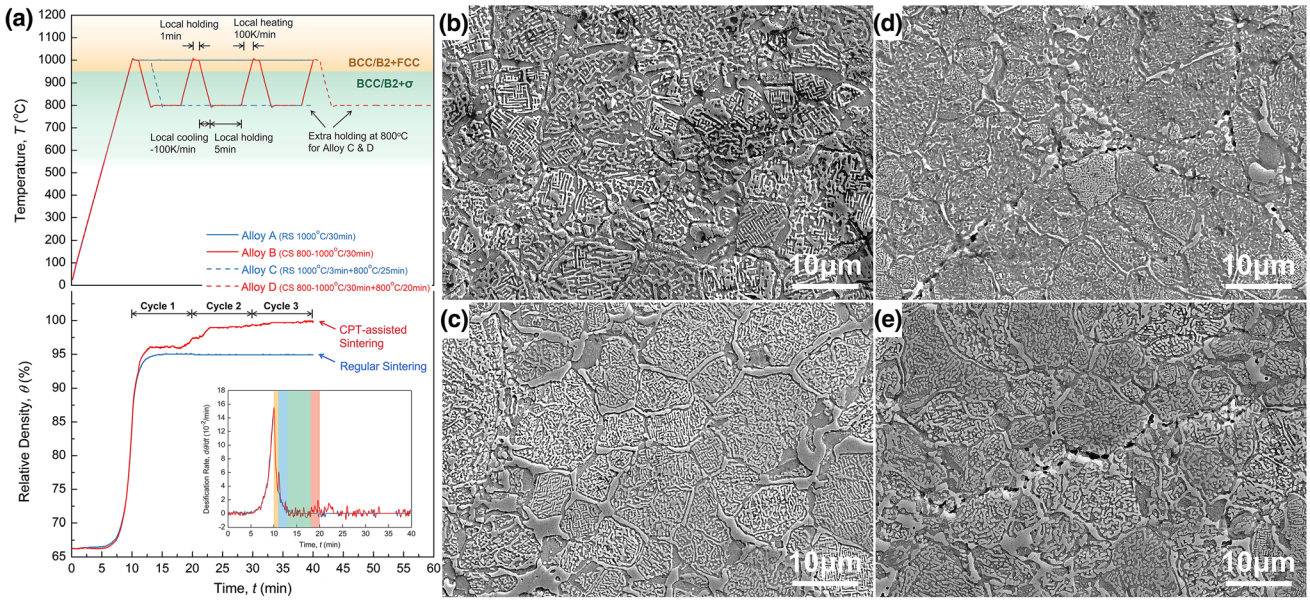


Fig. 3—Preparation routes and microstructures of AlCoCrFeNi CCAs: (*a*) the experimental temperature profiles of four sintered CCAs (upper) as well as the densification curves of typical sintered CCAs (Alloy A&B) (lower), insert is their corresponding densification rate curves (local hold stage at 1000 °C is marked yellow, local cooling stage is marked blue, local hold stage at 800 °C is marked green, local heating stage is marked red); (*b* through *e*) SEM images of four sintered CCAs: (b) Alloy A, (c) Alloy B, (d) Alloy C, and (e) Alloy D (Color figure online).

sintered CCAs. During the local holding stage at the lower-limit temperature (green portion), the insufficient sintering kinetics leads to the almost zero densification rate. In agreement with Figure 2(a), this local isothermal holding at 800 °C cannot bring an obvious densification due to it is not preferred sintering temperature for these CCAs. In addition, the precipitation of $\sigma$ phase does not happen during the cyclic phase transition process and accordingly make no contribution to the densification of Alloy A and B. This is because its formation requires long-time isothermal holding (like in Alloy C and D), which is inaccessible in fast CPT-assisted sintering process.

### B. *Phase Structure and Matrix Morphology of AlCoCrFeNi-Sintered CCAs*

The microstructure and phase structure of these CCAs generally can change with increasing the Al content, with BCC and FCC dual phase shown in this AlCoCrFeNi alloy.[41] It is noted that this closed-loop cyclic phase transition process does not change the phase composition of AlCoCrFeNi CCAs, as they all show the same FCC and BCC dual-phase peaks in XRD patterns for both Alloy A and B (Figure 4). Their $(111)_{FCC}$ and $(110)_{BCC}$ peak intensities are very close to each other as well, reflecting their similar FCC-to-BCC phase composition ratio. In addition, due to the disorder occupation of atoms in the crystal lattice, the difference in the lattice parameter (or lattice distortion) of each solid solution phase should be observed in these CCAs.

Thus, this leads to the asymmetry of peaks of these phases in the XRD patterns. However, the phase morphology undergoes a dramatic modification after CPT-assisted SPS process. The low-magnification EBSD phase maps in Figure 5 indicate that both alloys have BCC/B2 and FCC dual-phase structure, but it is more refined after CPT-assisted sintering. It is measured from the phase maps that these AlCoCrFeNi CCAs by regular sintering consist of 11.68 vol pct FCC and 88.31 vol pct BCC/B2 phase, while the CCAs by CPT-assisted sintering contain 12.25 vol pct FCC and 87.74 vol pct BCC/B2 phase. Typical microstructure is observed in AlCoCrFeNi CCAs prepared by regular sintering process (Figure 3(b)), which is previously reported in the same alloys by SPS at 1200 °C.[20] The irregular BCC phases are embedded in the B2 matrix grains to form a BCC/B2 interwoven structure. The FCC phase preferentially forms at BCC/B2 grain boundaries (GBs) in rod-like shape and exists in BCC/B2 matrix in a granular-like shape (Figure 5(b)). In contrast, the networked dendritic FCC phase is formed along the BCC/B2 grain boundaries in these CCAs after CPT-assisted sintering and the intragranular BCC/B2 morphology is obviously refined (Figure 3(c)). Moreover, the SEM micrographs indicate some residual pores in Alloys A after regular sintering, but a fully dense microstructure can be observed in Alloy B by CPT-assisted sintering. This agrees with the measured relative densities of alloys after sintering and is evidence showing the benefits of CPT process on densifying these CCAs. The granular-like FCC phase can be observed in alloy by CPT-assisted sintering (Figure 5(e)). Such microstructure is often seen in the AlCoCrFeNi CCAs casting ingots that are solidified from liquid state[42,43] at high temperature much above the melting point, but here it can be achieved *via* solid phase transition at lower temperature (Figure 6).

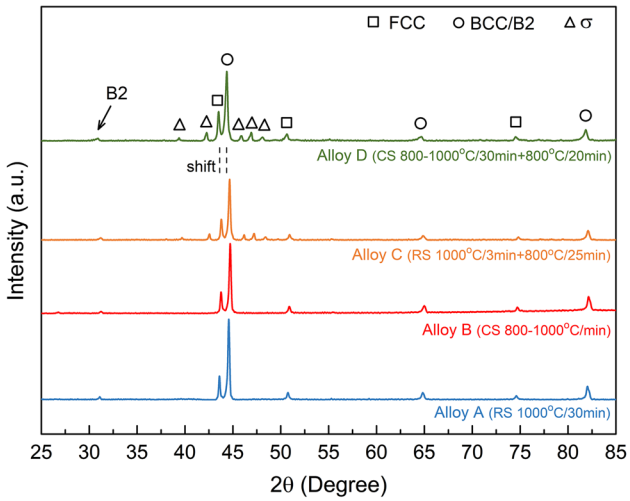


Fig. 4—The XRD patterns of four sintered AlCoCrFeNi CCAs.

The $\sigma$-phase precipitation (Figure 4) during extra long-time isothermal holding at 800 °C takes place in the regular sintered (Alloy C) and the CPT-assisted sintered CCAs (Alloy D). An obvious peak shift to the left is indexed in the XRD pattern of Alloy D, indicating that the FCC and BCC lattices in the AlCoCrFeNi CCAs after CPT processing are more likely to expand due to the $\sigma$-phase precipitation. Apart from some micro-pores at grain boundaries (GBs), extra isothermal holding also affects the intragranular BCC/B2 morphology of regular sintered CCAs (Figure 3(d)) but has little to no effect on that in CCAs after CPT-assisted sintering (Figure 3(e)). A small amount of dendritic FCC phase can be found in Alloy C, whereas the amount of dendritic FCC phase existing in Alloy D is much less than that in Alloy B without extra holding. This is perhaps because $\sigma$-phase precipitation is at the expense

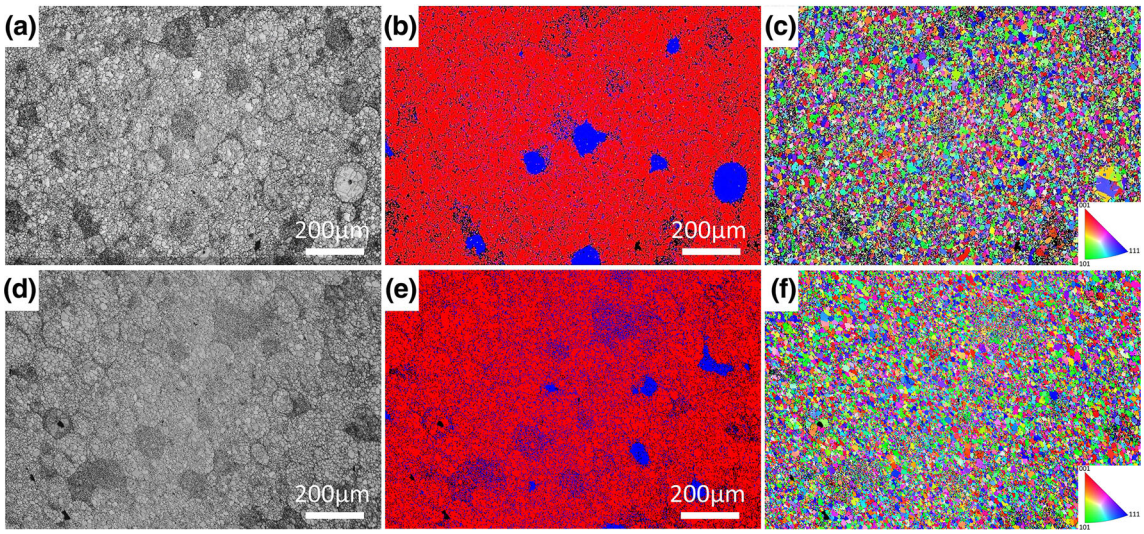


Fig. 5—Low-magnification EBSD images of AlCoCrFeNi CCAs by regular sintering (Alloy A) (*a* through *c*) and CPT-assisted sintering (Alloy B) (*d*) through (*f*): (a), (d) band contrast maps; (b), (*e*) phase maps with FCC in blue and BCC/B2 in red; (c), (f) crystal orientation maps (Color figure online).

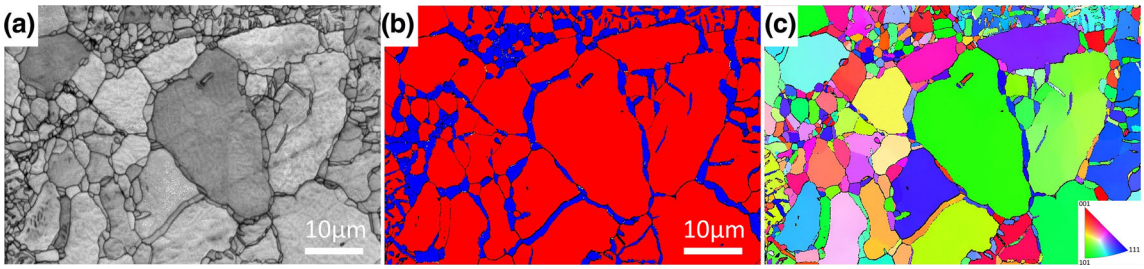


Fig. 6—The EBSD images of AlCoCrFeNi CCAs by CPT-assisted sintering (Alloy B): (*a*) band contrast maps; (*b*) phase maps with FCC in blue and BCC/B2 in red; (*c*) crystal orientation maps (Color figure online).

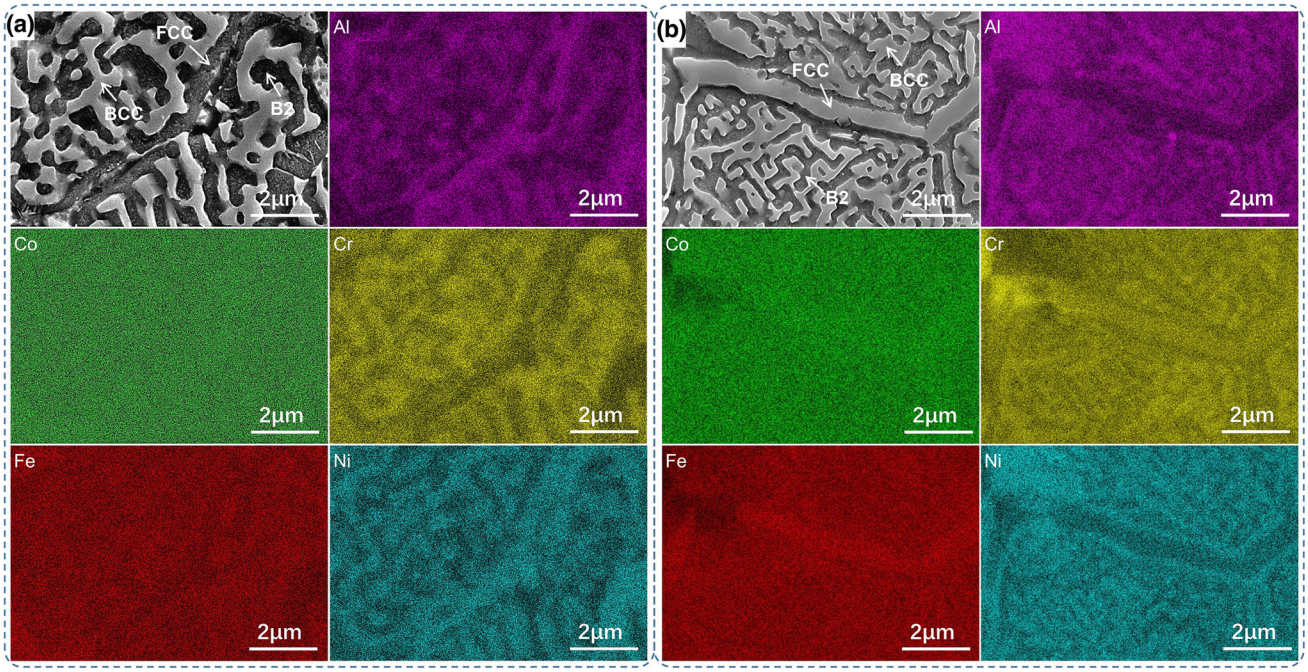


Fig. 7—High-magnification SEM images and corresponding EDS elemental mappings of AlCoCrFeNi CCAs: (*a*) Alloy A by regular sintering and (*b*) Alloy B by CPT-assisted sintering. Aluminum (purple); Cobalt (green); Chromium (yellow); Iron (red); Nickel (blue) (Color figure online).

of its decomposition during extra isothermal holding outside the FCC phase region.[32]

### C. *Grain Boundary (GB) Morphology of AlCoCrFeNi-Sintered CCAs*

The detailed GB morphologies of these CCAs after sintering are shown in Figure 7 with their corresponding EDS elemental maps. In the regular sintered AlCoCrFeNi CCAs (Figure 7(a)), no obvious structure but only a small amount of the concave FCC phase is found along the GBs. Co and Fe in Alloy A have uniform distribution. Al and Ni are enriched in the FCC and B2 phase, while Cr is enriched in BCC phase. Such element distribution feature is often seen in other AlCoCrFeNi CCAs.[44] In the CPT-assisted sintered CCAs (Figure 7(b)), there is a dendritic FCC phase continuously distributed along the GBs with a thickness of about 1 $\mu$m. Apparently, this dendritic FCC phase is Al/Ni-depleted and Cr-enriched, which is opposite to the case of Alloy A without CPT process. Co and Fe also tend to aggregate in the FCC phase. The element distribution inside the BCC/B2 grains is consistent with that of Alloy A. Considering the unaltered phase structure, the resulted composition redistribution behavior should occur within localized regions near the GBs in the CCAs after CPT-assisted sintering, which is crucial to the neck growth and shrinkage of powder materials during sintering. The detailed GB morphologies of AlCoCrFeNi CCAs with extra isothermal holding and their corresponding EDS mappings are given in Figure 8. Their elemental distribution shows similar characteristics to their corresponding alloys after the same sintering process but without extra isothermal holding. For Alloy C, Co and Fe are uniformly distributed within the alloy. Al/Ni are enriched in FCC and B2 phase, while Cr is enriched in BCC phase. However, Al is depleted in the $\sigma$-phase region. For Alloy D, the dendritic FCC phase is Al/Ni-depleted but Cr-enriched. Co and Fe also tend to aggregate at the

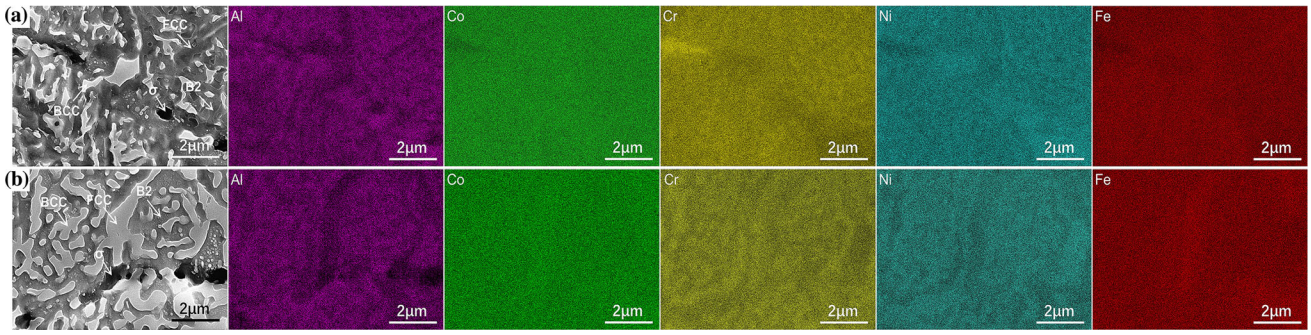


Fig. 8—High-magnification SEM images and corresponding EDS elemental mappings: (*a*) regular sintered AlCoCrFeNi CCAs with extra isothermal holding at 800 °C (Alloy C) and (*b*) CPT-assisted sintered AlCoCrFeNi CCAs with extra isothermal holding at 800 °C (Alloy D): Cobalt (green); Chromium (yellow); Iron (red); Nickel (blue) (Color figure online).

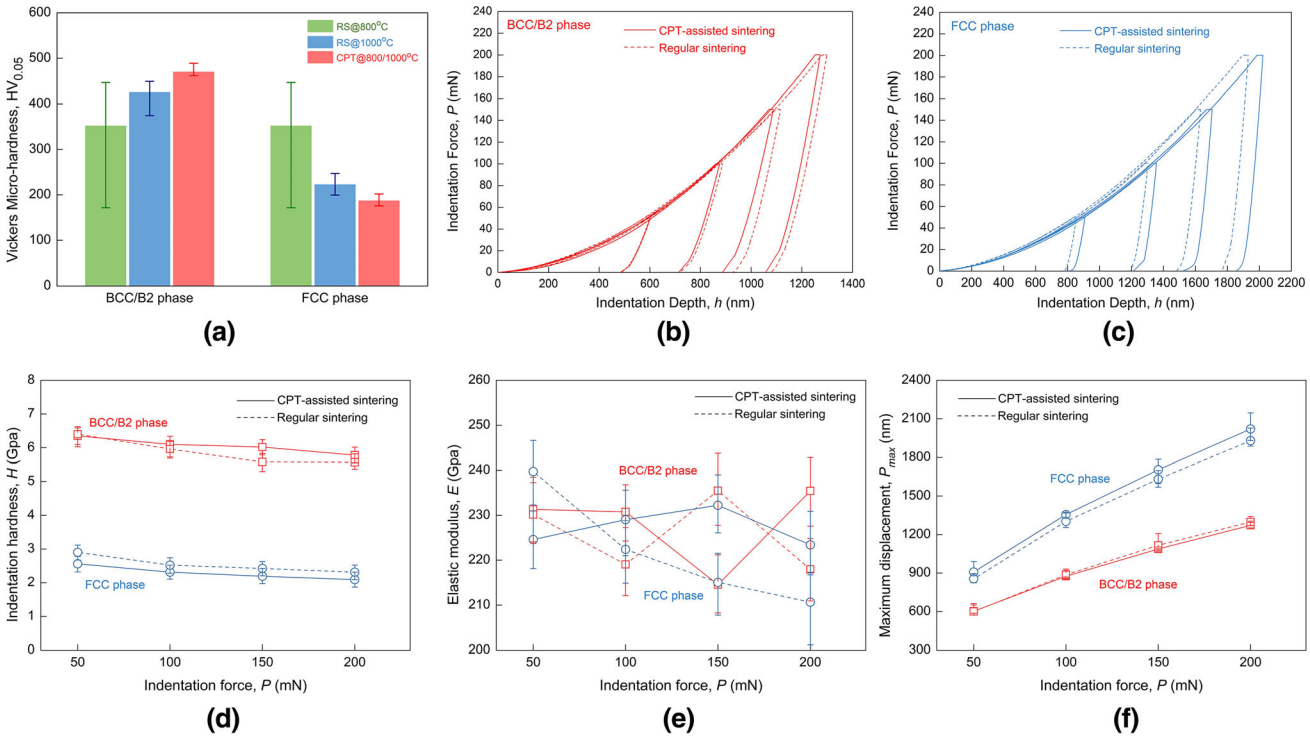


Fig. 9—Mechanical properties of BCC/B2 phase and FCC phase in AlCoCrFeNi CCAs prepared by regular sintering (RS) and CPT-assisted sintering (CPT): (*a*) Vickers hardness; (*b*) nano-indentation curves of BCC/B2 phase at different forces; (*c*) nano-indentation curves of FCC phase at different forces; (*d*) through (*f*) nano-indentation data of different phases in AlCoCrFeNi CCAs by different sintering method: (d) indentation hardness; (e) elastic modulus; and (f) maximum displacement. Each nano-indentation data is obtained from the average of nine repetitive measurements.

FCC phase, instead of being uniform. The depleted Al distribution is also found within the brittle $\sigma$-phase region in this alloy.

## D. *Mechanical Properties of AlCoCrFeNi Sintered CCAs*

The Vickers hardness of both BCC/B2 and FCC phases in AlCoCrFeNi CCAs prepared by different sintering method is shown in Figure 9(a) to clarify the CPT-assisted sintering as a promising method to prepare high-performance engineering CCAs. The regular sintering at 800 °C, due to the insufficient densification, results in a low average hardness of 353HV in the CCAs with large fluctuation. This is because of weak bonding causing the collapse of particles during loading. Apparently, in the densified dual-phase CCAs by regular sintering at 1000 °C, the BCC/B2 phase has a high Vickers hardness of 426HV, while the FCC has a low hardness of 224HV. It is interesting that the amplification of hardness difference between BCC/B2 phase (471HV) and FCC phase (188HV) can be observed in the alloy after CPT-assisted sintering.

The nano-indentation tests are conducted to compare the micro-mechanical properties of different phases in the AlCoCrFeNi CCAs prepared by two sintering

methods in detail. The representative nano-indentation curves of BBC/B2 phase (Figure 9(b)) and FCC phase (Figure 9(c)) are displayed with an applied force ranging from 50 to 200 mN. CPT-assisted sintering method obviously can provide an alternated mechanical behavior to the AlCoCrFeNi CCAs. The harder BCC/B2 phase with higher indentation hardness ($\Delta \sim 0.2$ GPa) but slightly lower maximum displacement is achieved after CPT-assisted sintering (Figures 9(d) and (f)), indicating the strengthened BCC/B2 matrix in these CCAs. The properties of the FCC phase are more significantly affected by applying CPT process, which shows a higher maximum displacement ($\Delta \sim 60$ nm) but a lower indentation hardness (Figures 9(d) and (f)). This indicates that the more ductile FCC phase is introduced in the alloy. The elastic modulus of these two phases do not show an obvious difference after the CPT process (Figure 9(e)), which is in favor of the simultaneous deformation of these two phases and can greatly reduce the risk of cracking or stress concentration at phase boundaries. In this AlCoCrFeNi CCAs, FCC phase is either distributed along the GBs in a rod-like shape or dispersed in the BCC/B2 matrix in granular-like shape. The combination of the best characteristics of BCC/B2 and FCC phase can lead to the presentation of good mechanical properties in these CCAs.[3,4] It is noted that many alloys can achieve their higher strength by lattice distortion effect or precipitation strengthening effect but at the expense of plasticity.[33,45,46] The capability of these CCAs to be a qualified engineering materials can be characterized by strengthened BCC/B2 matrix and toughened FCC phase along GBs, helping it to find more demanding application scenarios that requires comprehensive properties at high temperature.

## IV. DISCUSSION

### A. *Accelerated Densification in AlCoCrFeNi CCAs by Elemental Redistribution*

The EDS line scanning curves (Figure 10) taken across the phase boundaries of each sintered AlCoCrFeNi CCAs show their element redistribution. Unsurprisingly, the compositional differences across the GBs in CCAs prepared by regular sintering (Alloy A) are not significant. The CPT-assisted sintering process obviously amplifies the elemental redistribution behavior in the vicinity of GBs region in Alloy B, which is characterized by greater elemental composition differentiation between FCC and BCC/B2 phases. It should be noted that for both alloys, the time for isothermal holding or CPT process is the same (30 minutes). In Alloy A, no phase transition and temperature gradient takes place when the temperature reaches 1000 °C; therefore, the composition tends to be homogenized. However, when coupled with cyclic phase transition in Alloy B, the stimulus element diffusion and accelerated densification behavior can be achieved. The resulted chemical potential difference of elements in FCC and BBC/B2 phase during the grain boundary (or phase boundary) cyclic migration can cause such activated diffusion behavior. Due to the fast local heating/cooling rate during CPT process, it is believed that the caused element diffusion lags grain boundary migration. This amplified elemental redistribution phenomenon near GBs region can form in Alloy B. The $\sigma$-phase precipitation during extra isothermal holding brings more diffusion behavior in the alloy and leads to the formation of an Al-depleted region both in Alloy C and D; however, such $\sigma$-phase precipitation in Alloy D after CPT process causes the generation of more intensive element fluctuations phenomenon.

The oppositely alternated element distribution feature and the composition non-uniformity near grain (or phase) boundary indicate the activated diffusion behavior by CPT process, which can further contribute to the improved densification during SPS of AlCoCrFeNi CCAs. With this consideration, the primary outcome of such diffusion behavior is the result of Al/Ni migration into BCC/B2 phase and Co/Cr/Fe migration into FCC phase. The diffusion-based BCC/B2 and FCC phase transition processes are reversible during the sintering; however, the atom migration caused by CPT process lags grain boundary migration due to the fast local heating/cooling cycles. With these considerations, Figure 11 is a schematic diagram showing the possible diffusion behavior with one specific phase transition cycle. The white solid line in the figure represents the position of phase boundary (or GBs) before phase

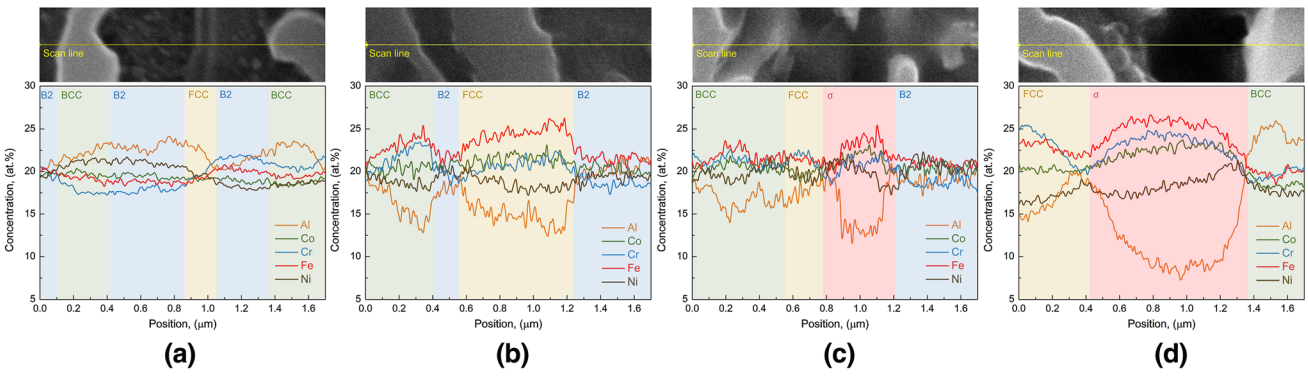


Fig. 10—The element distribution across the phase boundaries of four sintered AlCoCrFeNi CCAs by EDS line scanning: (*a*) Alloy A; (*b*) Alloy B; (*c*) Alloy C; and (*d*) Alloy D.

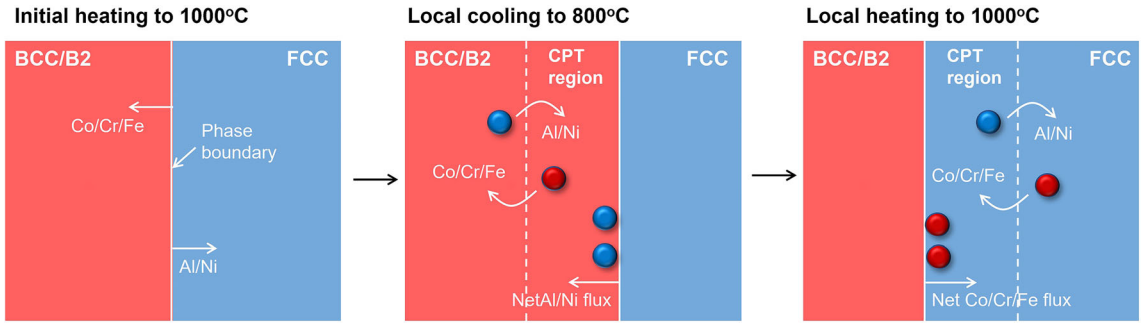


Fig. 11—Schematic diagram showing the elemental redistribution behavior during cyclic phase transition.

transition, and the white dash line represents the position of phase boundary after phase transition. Co/Cr/Fe atoms tend to transport into BCC/B2 phase, while Al/Ni atoms should transport into FCC phase during the isothermal holding process (Figure 7). However, shown in Figure 3(a), the local heating or cooling rate reaches 100 K/min, which is fast enough to promote the non-equilibrium phase transition and cause the hysteresis of atom diffusion to phase boundary migration. In the process of local cooling to 800°C, the migration of phase boundary towards FCC phase is faster than the diffusion of Al/Ni atoms into it, resulting in the reserve of Al/Ni atoms in CPT region (or a net diffusion flux of Al/Ni atoms into the BCC/B2 phase). Similarly, in the process of local heating to 1000 °C, the migration of phase boundary towards BCC/B2 phase is faster than the diffusion of Co/Cr/Fe atoms into it, resulting in the reserve of Co/Cr/Fe atoms in CPT region (or a net diffusion flux of Co/Cr/Fe atoms into the FCC phase). Therefore, during the CPT process, due to the hysteresis of element diffusion with respect to the non-equilibrium phase boundary migration, a net atomic diffusion flux is generated, and the improved diffusion behavior can be promoted.

### B. *Accelerated Densification in AlCoCrFeNi CCAs by Nano-grain Cluster*

The electron backscattered diffraction (EBSD) images in Figure 12 elaborate more details about the densification acceleration by CPT process in this AlCoCrFeNi CCAs. The granular FCC phase agglomerations can be found both in regular and CPT-assisted sintered CCAs, but some ring-like FCC phase agglomerations surrounding the BCC/B2 grains with internal misorientations are observed additionally in the alloy after CPT process. The band contrast map and grain orientation map indicate the generation of stress or deformation in the BCC/B2 phase during their CPT process. Interestingly, this stress here can promote the recrystallization and phase transformation, which lead to the formation of fine grain cluster near the phase boundary of CPT-assisted sintered CCAs. Phase maps show that this cluster is composed of BCC/B2 and FCC phase mixture with the grain sizes down to a few hundred nanometers. Generally, the grain refinement requires complex thermo-mechanical process or severe plastic deformation treatment, but here it can be achieved simply by thermal oscillation across the desired phase transition temperature. This nano-grain cluster should be in favor of better densification during sintering in many ways. The shorter path needed for lattice diffusion of atoms from the grain interiors to the grain boundaries leads to high amount of mass transfer. The massive GBs with high curvature and its gradient in this nano-grain cluster also promote a high grain boundary diffusion rate. In addition, as seen from the densification curve of AlCoCrFeNi CCAs (Figure 3(a)), the shrinkage can be activated during the cyclic phase transition process when compared with its absence in these CCAs at the holding stage during regular sintering. This indicates that the microstructure near the phase boundary region has been obviously softened during the CPT process. With such assistance, the significant sliding of these highly curved GBs can occur easily during the shrinkage of this CPT-assisted sintered CCAs at a high temperature, resulting in better superplasticity behavior that contributes to the desired densification acceleration.[23–25]

## V. CONCLUSION

In this work, spark plasma sintering coupled with cyclic phase transition process has been proposed for the efficient sintering of equiatomic AlCoCrFeNi complex concentrated alloys at low temperature. This new strategy can promote densification acceleration, microstructure modification, and properties improvement in these CCAs that are not available by regular sintering process. There are some major achievements that are summarized as follows:

(1) The CPT-assisted sintering of dual-phase AlCoCrFeNi CCAs can be developed by incorporating thermal cycles (800 °C to 1000 °C) across the BCC/B2 and FCC phase transition temperature (958 °C). The as-sintered dual-phase AlCoCrFeNi CCAs have a nearly full relative density that is unobtainable by regular sintering at lower-limit temperature (800 °C) and have an accelerated densification that is non-existent by regular sintering at upper-limit temperature (1000 °C). The higher densification rate is significantly shown in the local heating and local cooling stage of each

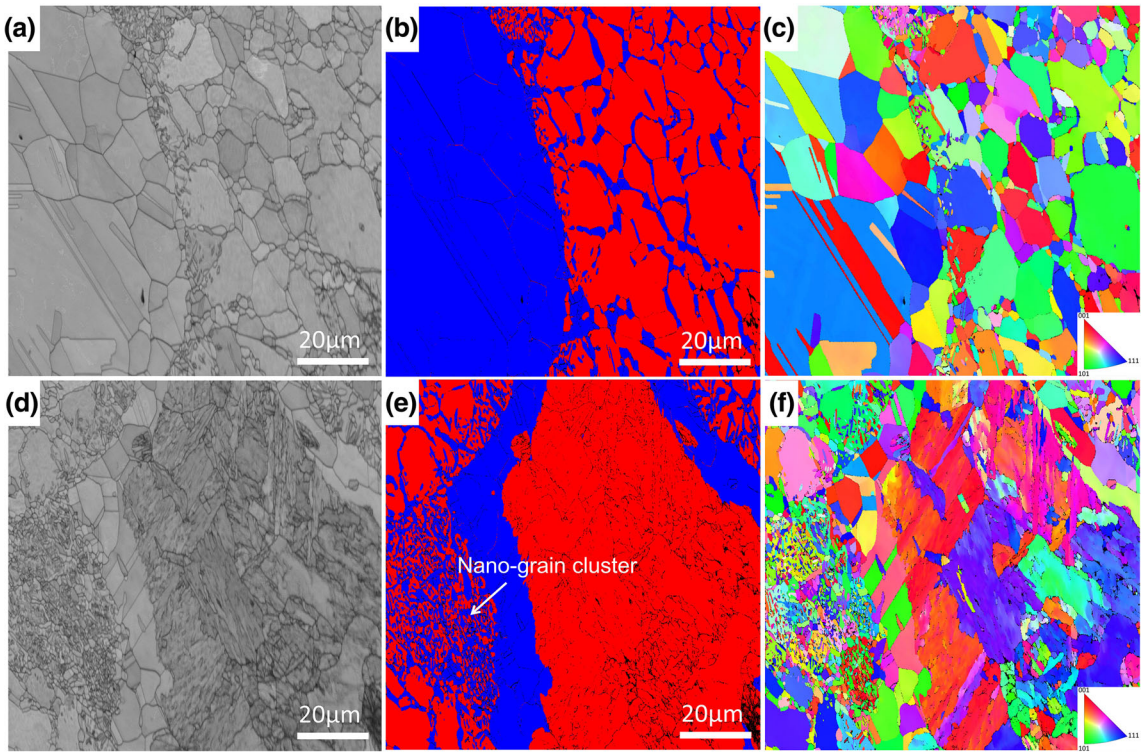


Fig. 12—The EBSD images in the featured areas of AlCoCrFeNi CCAs by regular sintering (Alloy A) (*a*) through (*c*) and CPT-assisted sintering (Alloy B) (*d*) through (*f*): (a), (d) band contrast maps; (*b*), (*e*) phase maps with FCC in blue and BCC/B2 in red; (*c*), (f) crystal orientation maps (Color figure online).

thermal cycle, which is attributed to the repetitive occurrence of phase transition.

(2) The application of CPT process can bring microstructure modification to the AlCoCrFeNi CCAs. The dendritic FCC phase with networked morphology is formed along the grain boundaries of BCC/B2 matrix in the CCAs after CPT-assisted sintering while the interwoven structure inside the intragranular BCC/B2 matrix is obviously refined as well. The CPT process also modifies the element distribution features in AlCoCrFeNi CCAs. The enriched Co/Cr/Fe elements and depleted Al/Ni elements are found in FCC phase, which are opposite in these CCAs by regular sintering.

(3) The CPT process also results in the improvement of mechanical properties of AlCoCrFeNi CCAs by facilitating the formation of hardened BCC/B2 phase and softened FCC phase. As a benefit of promoted diffusion between phases during CPT process, higher Vickers hardness of BCC/B2 phase 471HV and lower Vickers hardness of FCC phase 188HV than those by regular sintering can be achieved in the CCAs by CPT-assisted sintering. Higher indentation hardness of BCC/B2 phase (~ 0.2 GPa) and higher indentation displacement of FCC phase (~ 60 nm) also indicate the existence of properties differentiation of these two phases, which shows the potential of cyclic phase transition process in overcoming the strength–ductility trade-off in sintered CCAs.

(4) The acquisition of densification acceleration in this efficient CPT-assisted sintering is attributed to the elemental redistribution and the nano-grain cluster formation in AlCoCrFeNi CCAs. Due to the hysteresis of atomic diffusion during the CPT process, net diffusive flux of Al/Ni atoms to BCC/B2 phase and Co/Cr/Fe atoms to FCC phase promote the elemental redistribution behavior in the CCAs. The recrystallization during the CPT process also results in the formation of nano-grain clusters, which bring the densification acceleration *via* enhancing mass transfer and superplasticity behavior during sintering.

## ACKNOWLEDGMENTS

This work was supported by the National Science Foundation [Grant Number DMR-1900876]; and US Department of Energy, Basic Science Division, Materials Sciences Program [Grant Number DE-SC0022244].

## CONFLICT OF INTEREST

On behalf of all authors, the corresponding author states that there is no conflict of interest.

## REFERENCES


1. J.W. Yeh, S.K. Chen, S.J. Lin, J.Y. Gan, T.S. Chin, T.T. Shun, C.H. Tsau, and S.Y. Chang: *Adv. Eng. Mater.*, 2004, vol. 6, pp. 299–303.
2. B. Cantor, I.T.H. Chang, P. Knight, and A.J.B. Vincent: *Mater. Sci. Eng. A*, 2004, vol. 375, pp. 213–18.
3. W. Li, D. Xie, D. Li, Y. Zhang, Y. Gao, and P.K. Liaw: *Prog. Mater. Sci.*, 2021, vol. 118, 100777.
4. Z. Li, K.G. Pradeep, Y. Deng, D. Raabe, and C.C. Tasan: *Nature*, 2016, vol. 534, pp. 227–30.
5. B. Gludovatz, A. Hohenwarter, D. Catoor, E.H. Chang, E.P. George, and R.O. Ritchie: *Science*, 2014, vol. 345, pp. 1153–58.
6. P. Edalati, A. Mohammadi, Y. Li, H. Li, R. Floriano, M. Fuji, and K. Edalati: *Scripta Mater.*, 2022, vol. 209, 114387.
7. R. Bordia, S.J. Kang, and E.A. Olevsky: *J. Am. Ceram. Soc.*, 2017, vol. 100, pp. 2314–52.
8. P. Alvaredo, J.M. Torralba, and A. García-Junceda: *Encycl. Mater. Met. Alloys*, 2022, vol. 3, pp. 362–71.
9. T. Yang, Y.L. Zhao, Y. Tong, Z.B. Jiao, J. Wei, J.X. Cai, X.D. Han, D. Chen, A. Hu, and C.T. Liu: *Science*, 2018, vol. 362, pp. 933–37.
10. D.B. Miracle and O.N. Senkov: *Acta Mater.*, 2017, vol. 122, pp. 448–511.
11. M. Vaidya, K.G. Pradeep, B.S. Murty, G. Wilde, and S.V. Divinski: *Acta Mater.*, 2018, vol. 146, pp. 211–24.
12. M. Vaidya, S. Trubel, B.S. Murty, G. Wilde, and S.V. Divinski: *J. Alloys Compd.*, 2016, vol. 688, pp. 994–1001.
13. E.P. George, W.A. Curtin, and C.C. Tasan: *Acta Mater.*, 2020, vol. 188, pp. 435–74.
14. R.P. Baron, F.E. Wawner, and J.A. Wert: *Scripta Mater.*, 1998, vol. 39, pp. 269–75.
15. R. Haynes: *Powder Metall.*, 1971, vol. 14, pp. 64–70.
16. J.M. Zhu, H.M. Fu, H.F. Zhang, A.M. Wang, H. Li, and Z.Q. Hu: *Mater. Sci. Eng. A*, 2010, vol. 527, pp. 6975–79.
17. E.P. George, D. Raabe, and R.O. Ritchie: *Nat. Rev. Mater.*, 2019, vol. 4, pp. 515–34.
18. E.A. Olevsky and D.V. Dudina: *Field-Assisted Sintering: Science and Applications*, 1st ed. Springer, Cham, 2018, pp. 89–191.
19. A. Zhang, J. Han, J. Meng, B. Su, and P. Li: *Mater. Lett.*, 2016, vol. 181, pp. 82–85.
20. S. Xie, R. Li, T. Yuan, L. Zhou, M. Zhang, M. Wang, P. Niu, P. Cao, and C. Chen: *Mater. Charact.*, 2019, vol. 154, pp. 169–80.
21. Y. Xiao, X. Peng, and T. Fu: *Adv. Powder Technol.*, 2022, vol. 33, p. 103520.
22. C. Zhu, Z. Li, C. Hong, P. Dai, and J. Chen: *Int. J. Refract. Hard Met.*, 2020, vol. 93, p. 105357.
23. J. Han, B. Su, J. Lu, J. Meng, A. Zhang, and Y. Wu: *Intermetallics*, 2020, vol. 123, p. 106832.
24. J. Zhou, Y. Cheng, Y. Chen, and X. Liang: *Int. J. Refract. Hard Met.*, 2022, vol. 105, p. 105836.
25. S. Kohara: *Metall. Trans. A*, 1976, vol. 7A, pp. 1239–41.
26. O.A. Ruano, J. Wadsworth, and O.D. Sherby: *Metall. Trans. A*, 1982, vol. 13A, pp. 355–61.
27. C.A. Schuh and D.C. Dunand: *Acta Mater.*, 2002, vol. 50, pp. 1349–58.
28. C. Schuh, P. Noël, and D.C. Dunand: *Acta Mater.*, 2000, vol. 48, pp. 1639–53.
29. K. Li and F. Gao: *Adv. Powder Technol.*, 2018, vol. 29, pp. 3385–93.
30. E.J. Pickering, R. Muñoz-Moreno, H.J. Stone, and N.G. Jones: *Scripta Mater.*, 2016, vol. 113, pp. 106–09.
31. A. Karati, K. Guruvidyathri, V.S. Hariharan, and B.S. Murty: *Scripta Mater.*, 2019, vol. 162, pp. 465–67.
32. D. Karlsson, P. Beran, L. Riekehr, J. Tseng, P. Harlin, U. Jansson, and J. Cedervall: *J. Alloys Compd.*, 2021, vol. 893, p. 162060.
33. Z. Fu, A. Hoffman, B.E. MacDonald, Z. Jiang, W. Chen, M. Arivu, H. Wen, and E.J. Lavernia: *Acta Mater.*, 2019, vol. 179, pp. 372–82.
34. J.W. Kim, S.H. Kim, and Y.D. Kim: *Mater. Sci. Eng. A*, 2012, vol. 535, pp. 325–29.
35. J.W. Kim, S.Y. Song, and Y.D. Kim: *J. Alloy Compd.*, 2012, vol. 540, pp. 141–44.
36. S. Xie, R. Li, T. Yuan, M. Zhang, M. Wang, L. Yin, and P. Cao: *Mater. Charact.*, 2020, vol. 160, p. 110098.
37. K.R. Rao and S.K. Sinha: *Mater. Chem. Phys.*, 2020, vol. 256, p. 123709.
38. X. Zhang, J. Zhou, N. Lin, K. Li, K. Fu, B. Huang, and Y. He: *Int. J. Refract. Hard. Met.*, 2016, vol. 57, pp. 64–69.
39. X. Li, K. Hu, S. Qu, L. Li, and C. Yang: *Mater. Sci. Eng. A*, 2014, vol. 599, pp. 233–41.
40. K.Y. Tsai, M.H. Tsai, and J.W. Yeh: *Acta Mater.*, 2013, vol. 61, pp. 4887–97.
41. R. Sriharitha, B.S. Murty, and R.S. Kottada: *J. Alloy Compd.*, 2014, vol. 583, pp. 419–26.
42. C. Zhao, J. Li, Y. Liu, W.Y. Wang, H. Kou, E. Beaugnon, and J. Wang: *J. Mater. Sci. Technol.*, 2021, vol. 73, pp. 83–90.
43. K.S. Lee, B. Bae, J.H. Kang, K.R. Lim, and Y.S. Na: *Mater. Lett.*, 2017, vol. 198, pp. 81–84.
44. A. Manzoni, H. Daoud, R. Volkl, U. Glatzel, and N. Wanderka: *Ultramicroscopy*, 2013, vol. 132, pp. 212–15.
45. Z. Fu, L. Jiang, J.L. Wardini, B.E. MacDonald, H. Wen, W. Xiong, D. Zhang, Y. Zhou, T.J. Rupert, W. Chen, and E.J. Lavernia: *Sci. Adv.*, 2018, vol. 4, 8712.
46. B.E. MacDonald, Z. Fu, X. Wang, Z. Li, W. Chen, Y. Zhou, D. Raabe, J. Schoenung, H. Hahn, and E.J. Lavernia: *Acta Mater.*, 2019, vol. 181, pp. 25–35.